Accepted Manuscript

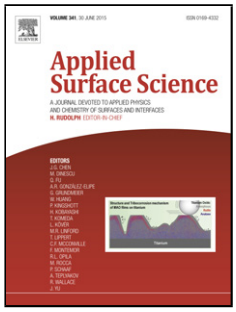

Title: A Primary Study into Graphene/Polyether Ether Ketone (PEEK) Nanocomposite for Laser Sintering

Authors: Binling Chen, Silvia Berretta, Ken Evans, Kaylie Smith, Oana Ghita

PII: S0169-4332(17)32874-X
DOI: https://doi.org/10.1016/j.apsusc.2017.09.226
Reference: APSUSC 37305

To appear in: *APSUSC*

Received date: 7-8-2017
Revised date: 21-9-2017
Accepted date: 26-9-2017

Please cite this article as: Binling Chen, Silvia Berretta, Ken Evans, Kaylie Smith, Oana Ghita, A Primary Study into Graphene/Polyether Ether Ketone (PEEK) Nanocomposite for Laser Sintering, Applied Surface Science https://doi.org/10.1016/j.apsusc.2017.09.226

A Primary Study into Graphene/Polyether Ether Ketone (PEEK) Nanocomposite for Laser Sintering

Binling Chen [*a], Silvia Berretta [a], Ken Evans [a], Kaylie Smith [b], Oana Ghita [a]

[a] College of Engineering, Mathematics and Physical Science, University of Exeter, Exeter, EX4 4QF, UK

[b] 2-DTech Limited, Unit 2, Chosen View Road, Cheltenham, GL51 9LT, UK

* Corresponding Author: B.Chen@exeter.ac.uk

Highlights

- Two methods of preparation of graphene/PEEK nanocomposite powders for Laser Sintering (LS) are proposed.
- The presence of graphene delays the start of the coalescence process by at least 10 s.
- Thin composite film is an attempt to replicate the thin layer formation of LS.
- The thermal stability, mechanical and electrical conductivity property can be enhanced with the addition of graphene.

Abstract

This paper proposes two methods of preparation of graphene/PEEK powders for Laser Sintering (LS) and investigates their behaviour in relation to their microstructure, the powder bed process and their properties. Thin composite films were fabricated in an attempt to replicate the thin layer formation of the powder bed process. Both methods of composite powder preparation (wet and dry) led to enhanced mechanical performance of the composite films at 0.1 and 0.5% graphene nano-platelets (GNP) concentrations. The TEM images show that the GNP act as a nucleation point in crystallisation of PEEK, being at the centre of the

spherulites. The hot stage microscopy revealed a 20 second delay in the onset of GNP/PEEK nanocomposite coalescence in comparison with plain PEEK. This is a very important observation for laser sintering, as it will influence the build strategy and specific parameters (e.g. time between layers deposition, multiple exposures). The excellent electrical conductivity properties of graphene were noticeable in the nanocomposite films at concentrations above 1 wt% GNP.

Keywords: Graphene, PEEK, Nanocomposites, Powders, Laser sintering

1. Introduction

As more polymeric materials are being developed for powder bed additive manufacturing [1, 2], the interest in multi-functionality through the addition of various fillers and nanoparticles is growing. The methods of introducing these fillers and nanoparticles into the plain polymeric powder and their impact on the properties of parts represent an important area of research. Aspects such as particles shape [3, 4], fillers interaction with the polymeric powder (agglomerating or acting as a flow aid) [5], cost-effectiveness of the method, or the health and safety [6, 7] of these nanocomposite powders requires better and more systematic research.

Melt compounding followed by milling is one of the most frequently used strategies of creating composite powders for Laser Sintering (LS) [8-10]. However, the success of this strategy is dependent on a combination of factors such as: 1) the polymeric material used; 2) the bulk density of the compounded material; and 3) the milling method employed. As previously shown in several studies [8-13], the milling process can significantly affect the shape, morphology and flow of the powder obtained. The bulk properties of a cryogenically

ground polyurethane powder were analysed and compared to a standard polyamide 12 LS material [10]. The authors found that their cryogenic milling method could not produce powders with suitable morphology for laser sintering [10]. High performance materials such as Polysulfone (PSU) and Polyether ether ketone (PEEK) have also been investigated and it was shown that it is possible to mill these materials to fine powders [8, 14]. Rotor milling could successfully produce PSU particles with the desired size (51.8 ± 15.2 μm) and morphology; but ball milling could cause severe degradation and only produce angular PSU particles well below the target size range [8]. In addition, two milling processes based on disc blades and rotatory cutting knives were applied for the fabrication of PEEK powders [14]. The rotary milling produced PEEK powders with superior properties in comparison with the disc milling method.

However, this strategy of melt compounding followed by milling, is highly energy intensive and therefore can become costly. Also, in some cases, excessive processing of the materials (either the polymer or the nanoparticle) can lead to changes in their structure and ultimate performance. For these reasons, the present study is investigating the performance of graphene/PEEK composite powders through a dry and wet method with minimum impact on the raw materials.

Wang et al. [15] used dry mixing for preparation of the PEEK/graphite platelets composites. They reported that the in-plane graphite platelets aligned along the X-Y plane and therefore improved the tensile strength [15]. PEEK with 5% graphite platelets composites exhibited the highest tensile strength comparing with the other samples in different graphite platelet percentages [15]. However, care should be taken when choosing to use the dry mixing method as the introduction of certain materials such as carbon fibres can lead to an alignment of the fibres in the x-y plane which can increase performance in the plane but present a significantly low performance in z direction [16, 17]. For example, CarbonMide, a

carbon fibre reinforced Polyamide 12 powders from EOS [18], has a tensile strength in x direction of 72 MPa, and y direction of 56 MPa. But the tensile strength in z direction is as low as 25 MPa [16]. These studies show that size, shape, and aspect ratio of matrix powder or reinforcement are very important in powder bed additive manufacturing processes. Wet methods based on dispersion of solids into liquids under ultra-sonication represent another way of preparation of composite powders. The ultrasonic cavitation generates high shear to break particle agglomerates [19]. Paggi et al. [20] reported the use of multiwalled carbon nanotubes (MWCNTs) into polyamide 12 powder through a wet method by ultrasound in chloroform. The materials exhibited enhanced mechanical properties with a limited amount of MWCNTs (1.70 %wt) [20].

2. Experimental

2.1 Materials

Victrex PEEK 150PF powders were supplied by Victrex UK [21]. The melting point of PEEK 150PF is 343 °C and the glass transition temperature is 143 ^{o}C. The typical processing temperature of PEEK 150PF is 380-400 °C [22]. 2-DTech Graphene Nano-Platelets (GNP) provided by Versarien UK [23]. These GNP flakes are below 10-layer carbon thickness.

2.2 Composite powder preparation

Two methods of preparation of the composite powders have been used; referred to in the paper as the wet and dry mix. In wet mixing, a suspension of GNP (0.1, 0.5, 1, 5, and 10 wt%, respectively) and ethanol was firstly ultrasonicated for 30 mins to allow a good dispersion of GNP into the solvent; PEEK150PF powder was added to

the GNP suspension, which was then subject to an additional sonication for another 30 mins. The suspension was further stirred on a hot plate (80 ^{o}C) for 2 hrs. The powders were left to deposit and solvent to evaporate and the final dry product was collected from the bottom of the beaker. For dry mixing, PEEK150PF powder and GNP (0.1, 0.5, 1, 5, and 10 wt%, respectively) were mixed by an EOS electric powder mixer for 6 hrs.

2.3 Film preparation

The mixed powders prepared by wet and dry mix were first spread evenly on a glass slide (Fisherbrand microscope slides, 0.8-1mm thickness), the layer of powder was heated and melted on a hotplate (V14160 Bibby HC500 hotplate) at 400 °C for 5 mins. Its thickness was controlled using an in-house built doctor blade rig. No glass cover was applied on top of the powder. The molten film on the glass slides was quickly transferred to another hot plate and isothermally crystallized at 300 °C for 30 mins [24].

2.4 Hot Stage Microscopy

Hot-stage microscopy was used to simulate the coalescence behaviour of nanocomposite powders in comparison with plain PEEK powders. Plain PEEK, 0.1% GNP/PEEK, and 1% GNP/PEEK (by weight) powders were spread on a microscope glass slide and then inserted into the hot-stage device. The powders were heated from room temperature up to 400 °C at a heating rate of 120 °C x min^{-1} and maintained for 2 mins. PEEK 150PF had a coalescence onset temperature of 340 °C, and the starting temperature was set at 320 °C.[25] Four tests were carried out for each material. The ratio of neck length (x) to the average particle diameter (D) of two particles (D1 and D2) was measured [25].

2.5 X-Ray Diffraction (XRD)

X-ray diffraction (XRD) patterns were recorded with a Cu Kα radiation (40 kV, and 40 mA) at a step time of 1 s and a step size of 0.03°. The lamellar thickness (*L*) of samples were calculated from Scherrer's Equation: $L = K\lambda/(FW_{(s)}\cos\Theta)$, where λ is the wavelength of the copper anode (λ = 0.154 nm), K is constant (K = 1) and $FW_{(s)}$ is the specimen peak broadening at half the maximum intensity (FWHM) in radians [24].

2.6 Scanning Electron Microscopy (SEM)

SEM images of the samples were recorded using a Philips XL-30 scanning electron microscope in a high vacuum mode and at an acceleration voltage of 20 kV. Samples were mounted using a conductive carbon double-sided tape. A thin (ca. 5 nm) coating of gold was sputtered onto the samples to reduce the effects of charging.

2.7 Transmission Electron Microscopy (TEM)

For TEM, the films were trimmed to the shape of a pyramid with the tip faced off to an area of approximately 0.3 x 0.3 mm. TEM samples with thicknesses of approximately 100 nm were sectioned in a microtone (Ultracut, Reichert-Jung, USA) from the pyramidal tip. The TEM specimens were placed on copper grids for analysis. The TEM images were captured using a Jeol JEM 1400 at an acceleration voltage of 120 kV.

2.8 Thermogravimetric analysis (TGA)

TGA was performed on one specimen per treatment using a Mettler-Toledo TGA/DSC1 Thermogravimetric Analyzer. The specimen (10 mg) was heated in an alumina crucible from 25 to 900 °C at 10 °C min^{-1} under air for thermal oxidative stability and air flow of 50 ml x min^{-1}.

2.9 Differential Scanning Calorimetry (DSC)

Thermal properties of powders were analysed by the Mettler Toledo DSC 821e/700 system. Samples of approximately 5mg were heated from room temperature to 400°C and cooled back to room temperature at a heating and cooling rate of 3°C x min^{-1} with nitrogen flow of 50 ml x min^{-1}. These testing settings are believed to better represent the cooling mechanism during the laser sintering process [25]. Evaluation of crystallinity content and crystallisation kinetics was performed using the crystallisation region of the DSC thermoscan in order to determine the crystallisation properties and infer the mechanical performance. Details of the analysis can be found elsewhere[26].

2.10 Raman spectra

Raman spectra of 2-DTech Graphene Nano-Platelets (GNP) were measured by He-Ne (632.8nm) laser using a Labram 300 system.

2.11 Mechanical test

Tensile testing experiments were performed using a LLOYD instrument EZ20 mechanical testing machine at room temperature (20 °C). The testing procedures detailed in the paper of Yuan et al., [24] were followed: The testing speed was equal to 20 mm x min^{-1} and the gauge length was 15 mm [24]. 20 samples were prepared and tested for pristine PEEK film and each of GNP/PEEK films. The stress at maximum load (MPa), percentage strain at maximum load, and their corresponding standard deviations were evaluated.

2.12 Resistivity measurements

The resistance was measured using a Keithley 616 Digital Electrometer. The tested samples measured 3 x 3 x 0.3 mm in size. The pressure applied on the tested samples is fixed

as 0.1 MPa at room temperature, as the resistance could be varied under different applied pressures and temperatures [27].

The electrical resistivity can be calculated from the following equation:

$$\rho = RA/L \qquad (1)$$

where ρ is the electrical resistivity, *R* is the measured resistance, *A* is the cross-sectional area of the specimen, and L is the length of the specimen. The electrical conductivity, σ, is the inverse of resistivity.

2.13 Surface measurements

The surface roughness of the GNP/PEEK films at 0.1 and 1wt% GNP was evaluated using a Taylor-Hobson Talyscan 150 surface profiler. Plain PEEK films were also tested for comparison. The average surface roughness (R_a) calculated from two individual linear measurements in a 2 mm × 2 mm selected surface area was scanned at 1000 μm x s^{-1} with spacing along the *Y*-axis of 5 μm. Two individual samples were measured for each film.

3. Results and discussion

3.1 Powder study

The Raman spectrum (Fig. 1) shows that the symmetry of the 2D band (~2700 cm^{-1}) is comparable with other reported few layer graphene materials [28]. This suggests that the graphene product is less than 10 layers in thickness. To evaluate the dispersion of GNP in the PEEK powders, SEM images were taken prior to film formation. It is shown that GNP is well dispersed amongst the PEEK particles under lower GNP weight percentage (0.1 and 1 wt%), but GNP tends to aggregate under higher concentrations (e.g. 10 wt%). The flat layers of GNP sheets in graphite can be observed in Fig. 2c and 2f. The two methods of composite powder preparation revealed that GNP "coats" the PEEK particles in both cases. The wet mixing method seems to provide a better dispersion of GNP and less aggregation due to the

ultrasonication process (see Fig. 2). The differences can be seen better at the higher concentrations of GNP.

Fig. 3a shows the % crystallisation over time for PEEK, 0.1, 1 and 10 wt% GNP/PEEK. Interestingly, PEEK and 0.1 wt% GNP/PEEK complete their crystallisation in 10 minutes, followed by 10 wt% GNP-PEEK completing it in 18 minutes and 1 wt% GNP-PEEK in 22 minutes. The fact that PEEK and 0.1 wt% GNP/PEEK show a crystallisation time within the same time interval means that 0.1 wt% GNP/PEEK powder can be processed in laser sintering using similar settings as PEEK. It can be noted that the higher loading of GNP in PEEK slows down the crystallisation mechanism by 2.5 minutes although achieves the highest % crystallisation. These observations are very important for the cooling phase and the overall build duration of the laser sintering process. Fig. 3b shows the rate of crystallisation for the plain PEEK and the three GNP/PEEK grades selected in Fig 3a. The first derivative curves show that 0.1 wt% GNP/PEEK start to crystallize earlier than PEEK; while 10 wt% GNP/PEEK has the slowest rate of crystallisation.

The particle coalescence of 1wt% GNP/PEEK and 10wt% GNP/PEEK is shown in Fig. 4 and 5, respectively. The black dots noticed on the surface of the melted, translucent particles represent the graphene nanoplatelets. The ratio x/D of the measured powders is plotted against the neck formation time (Fig. 6). Fig 6a to 6c show the coalescence process of GNP/PEEK particles at 0.1, 1 and 10 wt% GNP. For each GNP/PEEK concentration presented in Fig 6, three repeats were included to show the variation recorded throughout the test and measurement. Compared with PEEK powders, GNP/PEEK particles exhibit a different curve shape, the initial part of the coalescence process is slower followed by a faster change in neck growth. This change could be due to the thermal conductive property of the GNP in the PEEK particles. This observation is consistent with our previous work on encapsulated carbon fibre (Cf) and carbon black (CB) poly aryl ether ketones (PAEK) powders [14]. When comparing the neck growth plots of GNP/PEEK of different concentrations in Fig. 6d, there wasn't a clear correlation between the increase of % GNP and the start and rapid increase in neck growth. However, based on previous results on Cf and CB and results presented here in Fig. 6a-c, it can be concluded that the presence of carbon micro and nano fillers delays the start of the coalescence process by at least 10 s. This is a very important observation for laser sintering, as new build strategies will have to be set up to consider such delays during layer by layer deposition. **3.2 GNP/PEEK film study**

For a comparative study, thin-film samples (250 μm thick) of PEEK and GNP/PEEK composite fabricated using the wet and dry dispersion methods were prepared and fully characterised for their mechanical, thermal, and electrical properties.

In Fig. 7, the peaks at 18.8 °, 20.8 °, 22.8 °, and 28.9 ° can be attributed to the PEEK crystal planes 110, 111, 200, 211 [29]. The XRD data shows also the graphitic peak of GNP at 26.3 °; attributed to the (002) planes of GNP [30]. This typical peak of GNP was present in all composites compositions. No new peaks appeared, indicating that no significant reaction happened between PEEK and GNP during melting and crystallisation phases. The intensity of GNP peak increased with the increase of GNP. Analysis into the polymer crystal morphology showed that based on the peak position of crystal planes and full width at half maximum intensity (FWHM), the lamellar thickness varied between 13 and 15 nm (shown in Table S1). These results show that the amount of GNP does not affect the lamellar thickness significantly.

Fig. 8 shows the SEM images of the surfaces of PEEK and GNP-PEEK composite films obtained through simple hot melting of the powder. It can be seen from Fig. 8a that the surface of plain PEEK (S0) is flat but with some small defects and cavities. The sample S1-wet (Fig. 8c) has the similar surface morphology as PEEK (S0). Interestingly, S0.1-wet (Fig. 8b) shows much smoother surface compared to that of pure PEEK and S1-wet, with less voids and cavities. The wt% GNP influences the surface roughness of the film, an important parameter for this study and its potential use as a laser sintering feedstock material. Interactions between GNPs and PEEK particles can lead to cavities and surface imperfections further affecting the mechanical and electrical properties of films. Surface roughness tests measured by means of Talyscan have been carried out to confirm the SEM observations. The surface roughness results are shown in Table 1.

The S0.1-wet samples have the lowest R_a value indicating the smoothest surface. The surface morphology shows that the presence of GNP flakes helps heat conduction through the film and formation of smoother surfaces. This is specifically improved at 0.1wt% GNP due to

possibly good GNP dispersion and interaction with the PEEK particles. At a higher wt% GNP, such as 1wt%, the nanoparticles start to agglomerate and therefore lead to a rougher surface.

The dry-mixed films, S0.1-dry and S1-dry (Fig. 8d and e) present rough surfaces with voids and cavities. The wet method allowed the GNP flakes to adhere better to the PEEK particles than the dry mixing. In addition, the introduction of the GNP through dry mixing might have changed the permeability of the powder and created a less dense composite powder. Berretta et al., noticed that there is a good correlation between the quality of the powder (morphology and flow) and the surface roughness of 10 layers of sintered powder [31]. Poor powder flow led to a rougher surface with pores and cavities.

For a detailed morphological study of GNP-PEEK nanocomposites, Fig. 9 shows the TEM images of the microtome-cut S0.1-wet and S5-wet films. As shown in Fig. 9a, spherulitic crystal structure can be observed in S0.1-wet, which is in consistent with the pure PEEK [32]. GNPs were homogeneously dispersed in the matrix and in many cases the GNP were located in the centre of crystal, presumably acting as nucleation point during crystallization. Rong et al. suggested carbon nanotubes had the similar function for PEEK [33]. Under high magnification (Fig. 9b), thin layers of GNP embedded into matrix can be observed. While for S5-wet, the GNP were randomly oriented and dispersed into the PEEK matrix (Fig. 9c). At high concentrations, the GNP tend to fold and aggregate together because of its high loading (Fig. 9d). The S0.1-dry and S5-dry films (Fig. 9g and h) exhibit similar morphology to S0.1-wet and S5-wet films.Thermal oxidative stability of studied materials was measured by TGA. As shown in Fig. 10, the thermal oxidative decomposition of PEEK is a two-step process [34]. The GNP/PEEK composites exhibited a similar two-step process. The first step of thermal decomposition can be attributed to the random chain scission of the ether and ketone bonds [35, 36], while the second decomposition step can be attributed to thermal oxidisation of all the carbonaceous material [34]. The onset of thermal oxidative decomposition for all studied materials is similar, 540°C. All composite materials and plain PEEK grade lost approximately 30 % weight in the first stage of thermal oxidative decomposition. The difference between the concentrations of GNP/PEEK appears in the second stage possibly due to the oxidation of GNP. A possible explanation is that GNP with lower content (≤1 wt%) promotes the oxidative decomposition, as GNP are thermally conductive thus enhancing the heat adsorption; but GNP with higher content (≥ 5 wt%) could retard the oxidative decomposition, due to its high thermal stability [37, 38].The typical stress-strain curves obtained from the PEEK and GNP-PEEK nanocomposites are presented in Fig. 11. It shows that GNP can improve the mechanical properties of PEEK and the level of reinforcement

depends on the GNP content and powder mixing method. Fig. 12 shows the stress at maximum load and percentage strain at maximum load. The pure PEEK has a stress at maximum load of 82.6 ± 16.8 MPa. For wet mixed samples, the addition of 0.1%, 0.5% and 1% GNP led to 17%, 23%, and 12% increase in stress at maximum load. The dry mixed samples had a 25%, 21%, and 9% increase in stress for the same GNP concentrations: 0.1; 0.5 and 1%. However, a further increase of GNP to 5 wt% GNP led to a reduction of up to 48%. As generally noticed in many studies, the introduction of nanomaterials and fillers tends to lead to a decrease in ductility. However, in this study, at low loadings of GNP (0.1 wt% and 0.5 wt%), the percentage strain at maximum load was increased up to 33%. In addition, the toughness of S0.1-dry had an increase of up to 38%. These results are consistent with the study of Wang *et al.,* where the authors reported GNP are efficient in toughening polymers at significant low loadings [39]. Similarly, Díez-Pascual et al., [40] reported an increase in toughness of PEK/CNT (polyether ketone/carbon nanotube) composites at low loadings, when compatibilising agents and covalent grafting strategies had been used. Fig. 13 shows the SEM images of the fractured surfaces of PEEK and GNP-PEEK nanocomposites. The neat PEEK (Fig. 13a) shows the spherulitic crystal structure as well as the granular blocks previously noticed by Wang et al. [24, 32]. Fig. 13c shows the presence of partially pulled out GNP out of the matrix. This is an indication of weak interfacial bonding between the GNP and PEEK matrix, which results in low stress transfer and weak mechanical performance. The GNP used here did not receive any surface treatment. Potentially, an appropriate chemical treatment of GNP could improve the adhesion and wetting characteristics. Previous studies on CNT/PEEK composites showed that polymer grafting can be effective in improving dispersion and mechanical properties [40, 41].

As graphene is known for its remarkable electron mobility, the electrical resistivity and conductivity of these composite films was tested and results are shown in Table 2. As expected, the electrical resistivity decreases significantly with the increase of GNP %. As an insulator, the neat PEEK film (S0) has a high electrical resistivity of $3.9 \pm 1.4 * 10^{9}$ Ω·m. For the composite films prepared using the wet method, the electrical resistivity reduces from $1.4 \pm 0.2 * 10^{9}$ to 2.2 ± 0.1 Ω·m with the addition of GNP from 0.1 wt% to 10 wt%, while the electrical resistivity of films prepared through the dry mix, has values decreasing from $2.5 \pm 0.2 * 10^{9}$ to 2.3 ± 0.1 Ω·m with the addition of GNP from 0.1 wt% to 10 wt%. It worth noting that there is a sharp change in electrical performance between 1 and 5 wt% GNP. It is possible that the GNP weight fraction required to reach the percolation threshold is within 1-5 wt% GNP.

In summary, Fig. 14 illustrates the changes in electrical resistivity, conductivity, stress and strain as a function of wt% GNP. The shaded regions represent the areas where GNP concentration gives the best performance for a specific property.

The results in Fig. 14 clearly show that depending on the property required, different wt% GNPs need to be added. In order for the GNPs to act as mechanical reinforcement, a concentration of 0.1 to 0.5 % wt is optimal. The SEM images of the nanocomposite powders and the films show a better dispersion and better adhesion of the GNP on the PEEK particles, as well as a smoother surface at 0.1wt% GNP, which is in agreement with the enhanced mechanical performance noticed in the films. In contrast, the 5 to 10 wt% GNP led to a decrease in tensile strength but enhanced significantly the electrical conductivity. The crystallinity results and coalescence data although not directly related with the above properties are important when using nanocomposite powders for laser sintering. For example, knowing the crystallisation behaviour of the nanocomposites at different wt% GNP helps to define the optimum bed temperature in the laser sintering system. In addition, the higher loading of GNPs led to the faster neck growth but delayed the start of the crystallization as shown by other studies [14].

4. Conclusions

The fabrication of nano composite powders for laser sintering processes is an exciting route towards manufacture of lightweight structures with added functionalities. This paper presented two potentially cost effective preparation methods of GNP/PEEK powders. The SEM images show the homogeneous dispersion of GNP in the PEEK matrix under low GNP

concentration (0.1 wt%). TEM images show that the GNP are at the centre of the spherulites, acting as a nucleation point during the crystallisation of PEEK. The hot stage microscopy highlighted a 10 to 20 second delay in the onset of GNP/PEEK nanocomposite coalescence compared with the plain PEEK, which is an important observation for laser sintering. Unfortunately, the optimum wt% GNP differs for the different tested properties and so there is no on specific optimum wt%. The thin films exhibited enhanced mechanical properties within 0.1 - 0.5 %wt GNP, whereas the electrical conductivity properties of the composite films were significantly improved by the addition of GNP within 1 - 5 %wt GNP. This study provides a guide into nanomaterials properties required for laser sintering and defines methodologies suitable for understanding nanocomposite powders for laser sintering.

Acknowledgements

The authors would like to thank the UK Engineering and Physical Science Research Council for its funding (EPSRC grant no EP/L017318/1-Particle Shape and Flow behaviour in Laser Sintering: from modelling to experimental validation), 2D-Tech for providing the graphene and John Benson for his help with the Raman evaluation.

References

[1] M. Schmid, A. Amado, K. Wegener, Polymer powders for selective laser sintering (SLS), AIP Conf. Proc., 1664 (2015) 160009.
[2] A.C. de Leon, Q. Chen, N.B. Palaganas, J.O. Palaganas, J. Manapat, R.C. Advincula, High performance polymer nanocomposites for additive manufacturing applications, React. Funct. Polym., 103 (2016) 141-155.
[3] E.J.R. Parteli, T. Pöschel, Particle-based simulation of powder application in additive manufacturing, Powder Technol., 288 (2016) 96-102.

[4] M. Schmid, A. Amado, K. Wegener, Materials perspective of polymers for additive manufacturing with selective laser sintering, J. Mater. Res., 29 (2014) 1824-1832.
[5] K. Wudy, L. Lanzl, D. Drummer, Selective Laser Sintering of Filled Polymer Systems: Bulk Properties and Laser Beam Material Interaction, Physics Procedia, 83 (2016) 991-1002.
[6] B. Stephens, P. Azimi, Z. El Orch, T. Ramos, Ultrafine particle emissions from desktop 3D printers, Atmos. Environ., 79 (2013) 334-339.
[7] B.T. Wittbrodt, A.G. Glover, J. Laureto, G.C. Anzalone, D. Oppliger, J.L. Irwin, J.M. Pearce, Life-cycle economic analysis of distributed manufacturing with open-source 3-D printers, Mechatronics, 23 (2013) 713-726.
[8] N. Mys, R. Van De Sande, A. Verberckmoes, L. Cardon, Processing of Polysulfone to Free Flowing Powder by Mechanical Milling and Spray Drying Techniques for Use in Selective Laser Sintering, Polymers, 8 (2016) 150.
[9] N. Mys, A. Verberckmoes, L. Cardon, Processing of Syndiotactic Polystyrene to Microspheres for Part Manufacturing through Selective Laser Sintering, Polymers, 8 (2016) 383.
[10] R.D. Goodridge, M.L. Shofner, R.J.M. Hague, M. McClelland, M.R. Schlea, R.B. Johnson, C.J. Tuck, Processing of a Polyamide-12/carbon nanofibre composite by laser sintering, Polym. Test., 30 (2011) 94-100.
[11] E. Ivanov, C. Suryanarayana, Materials and Process Design through Mechanochemical Routes, J. Mater. Synth. Process., 8 (2000) 235-244.
[12] D.L. Zhang, Processing of advanced materials using high-energy mechanical milling, Prog. Mater Sci., 49 (2004) 537-560.
[13] S. Ziegelmeier, F. Wöllecke, C. Tuck, R. Goodridge, R. Hague, Characterizing the bulk & flow behaviour of LS polymer powders, in: Proceedings SFF Symposium, Austin (TX), USA, 2013.
[14] B. Chen, Y. Wang, S. Berretta, O. Ghita, Poly Aryl Ether Ketones (PAEKs) and carbon-reinforced PAEK powders for laser sintering, J. Mater. Sci., (2017) 1-16.
[15] Y. Wang, D. Rouholamin, R. Davies, O.R. Ghita, Powder characteristics, microstructure and properties of graphite platelet reinforced Poly Ether Ether Ketone composites in High Temperature Laser Sintering (HT-LS), Mater. Des., 88 (2015) 1310-1320.
[16] Carbonmide, https://3dfabriek.nl/carbonmide-3d-printen/, in, 2016.
[17] A. Jansson, L. Pejryd, Characterisation of carbon fibre-reinforced polyamide manufactured by selective laser sintering, Addit. Manuf., 9 (2016) 7-13.
[18] EOS, http://www.eos.info/material-p, in 2016.
[19] B. Bittmann, F. Haupert, A.K. Schlarb, Ultrasonic dispersion of inorganic nanoparticles in epoxy resin, Ultrason. Sonochem., 16 (2009) 622-628.
[20] R.A. Paggi, V.E. Beal, G.V. Salmoria, Process optimization for PA12/MWCNT nanocomposite manufacturing by selective laser sintering, Int. J. Adv. Manuf. Tech, 66 (2013) 1977-1985.
[21] Victrex, https://www.victrex.com/en/, in 2016.
[22] V.P. 150PF, https://www.victrex.com/~/media/datasheets/victrex_tds_150pf.pdf, in, 2016.
[23] Versarien, http://www.2-dtech.com/products/, in, 2016.
[24] Y. Wang, B. Chen, K.E. Evans, O. Ghita, Novel fibre-like crystals in thin films of Poly Ether Ether Ketone (PEEK), Mater. Lett., 184 (2016) 112-118.
[25] S. Berretta, Y. Wang, R. Davies, O.R. Ghita, Polymer viscosity, particle coalescence and mechanical performance in high-temperature laser sintering, J. Mater. Sci., 51 (2016) 4778-4794.
[26] T. Liu, Z. Mo, S. Wang, H. Zhang, Nonisothermal melt and cold crystallization kinetics of poly(aryl ether ether ketone ketone), Polym. Eng. Sci,, 37 (1997) 568-575.

[27] M. Mohiuddin, S. Van Hoa, Electrical resistance of CNT-PEEK composites under compression at different temperatures, Nanoscale Res. Lett., 6 (2011) 419.
[28] A.C. Ferrari, Raman spectroscopy of graphene and graphite: Disorder, electron–phonon coupling, doping and nonadiabatic effects, Solid State Communications, 143 (2007) 47-57.
[29] P.C. Dawson, D.J. Blundell, X-ray data for poly(aryl ether ketones), Polymer, 21 (1980) 577-578.
[30] B. Yazdani, Y. Xia, I. Ahmad, Y. Zhu, Graphene and carbon nanotube (GNT)-reinforced alumina nanocomposites, J. Eur. Ceram. Soc., 35 (2015) 179-186.
[31] S. Berretta, K.E. Evans, O. Ghita, Processability of PEEK, a new polymer for High Temperature Laser Sintering (HT-LS), Eur. Polym. J., 68 (2015) 243-266.
[32] Y. Wang, J.D. Beard, K.E. Evans, O. Ghita, Unusual crystalline morphology of Poly Aryl Ether Ketones (PAEKs), RSC Adv., 6 (2016) 3198-3209.
[33] C. Rong, G. Ma, S. Zhang, L. Song, Z. Chen, G. Wang, P.M. Ajayan, Effect of carbon nanotubes on the mechanical properties and crystallization behavior of poly(ether ether ketone), Compos. Sci. Technol., 70 (2010) 380-386.
[34] P. Patel, T.R. Hull, R.E. Lyon, S.I. Stoliarov, R.N. Walters, S. Crowley, N. Safronava, Investigation of the thermal decomposition and flammability of PEEK and its carbon and glass-fibre composites, Polym. Degrad. Stab., 96 (2011) 12-22.
[35] P. Patel, T.R. Hull, R.W. McCabe, D. Flath, J. Grasmeder, M. Percy, Mechanism of thermal decomposition of poly(ether ether ketone) (PEEK) from a review of decomposition studies, Polym. Degrad. Stab., 95 (2010) 709-718.
[36] L.H. Perng, C.J. Tsai, Y.C. Ling, Mechanism and kinetic modelling of PEEK pyrolysis by TG/MS, Polymer, 40 (1999) 7321-7329.
[37] A.E. Galashev, O.R. Rakhmanova, Mechanical and thermal stability of graphene and graphene-based materials, Phys. Usp., 57 (2014) 970.
[38] L. Yang, S. Zhang, Z. Chen, Y. Guo, J. Luan, Z. Geng, G. Wang, Design and preparation of graphene/poly(ether ether ketone) composites with excellent electrical conductivity, J. Mater. Sci., 49 (2013) 2372-2382.
[39] X. Wang, M. Song, Toughening of polymers by graphene, Nanomater. Energy, 2 (2013) 265-278.
[40] A.M. Díez-Pascual, M. Naffakh, C. Marco, G. Ellis, M.A. Gómez-Fatou, High-performance nanocomposites based on polyetherketones, Prog. Mater Sci., 57 (2012) 1106-1190.
[41] A.M. Diez-Pascual, G. Martinez, M.T. Martinez, M.A. Gomez, Novel nanocomposites reinforced with hydroxylated poly(ether ether ketone)-grafted carbon nanotubes, J. Mater. Chem., 20 (2010) 8247-8256.

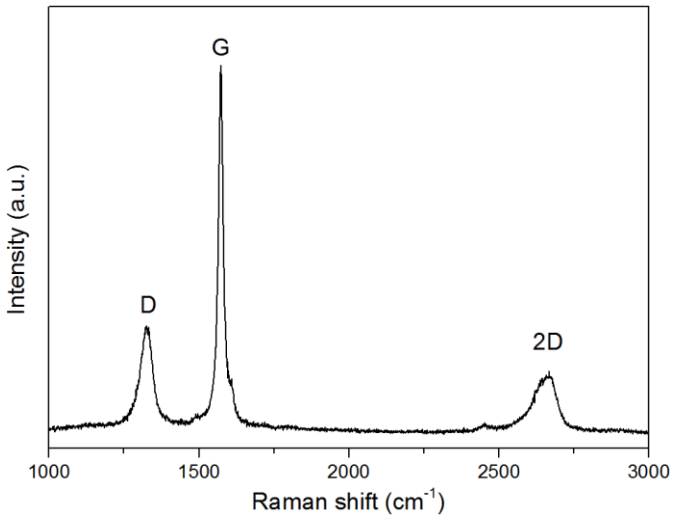

Fig 1. Typical Raman spectrum of 2-DTech Graphene Nano-Platelets (GNP).

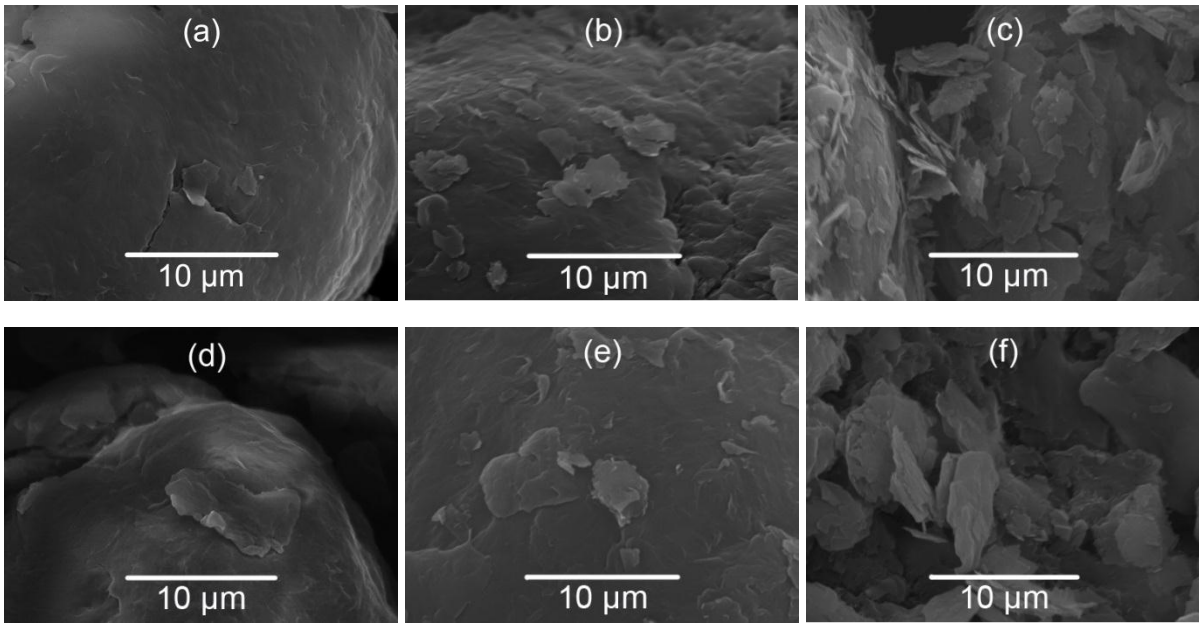

Fig 2. SEM images of (a) 0.1wt% GNP/PEEK powder, (b) 1wt% GNP/PEEK powder, and (c) 10wt% GNP/PEEK powder created using the wet method; (d) 0.1wt% GNP/PEEK powder, (e) 1wt% GNP/PEEK powder, and (f) 10wt% GNP/PEEK powder obtained using the dry method.

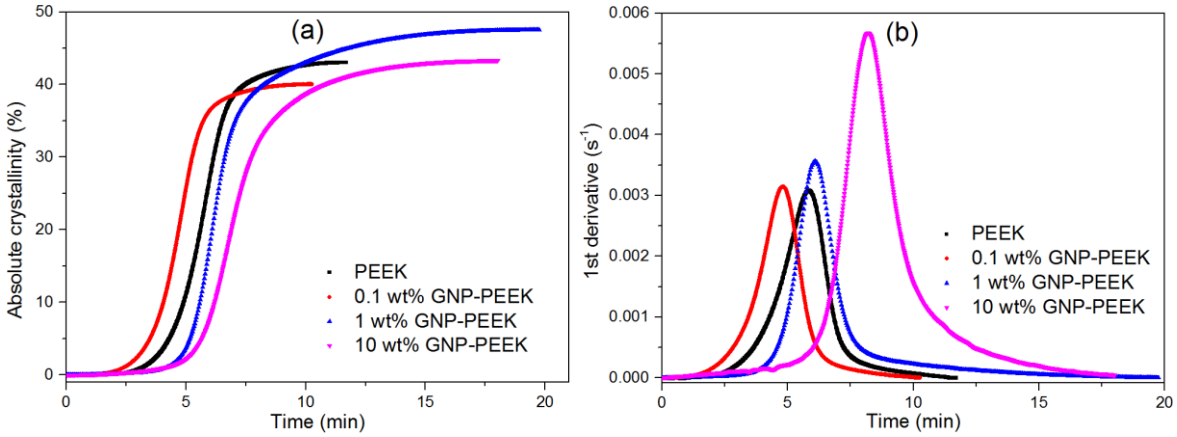

Fig 3. (a) % Crystallinity vs time (b) rate of crystallisation vs time of PEEK, 0.1,1, and 10 wt% GNP/PEEK particles created using the wet method.

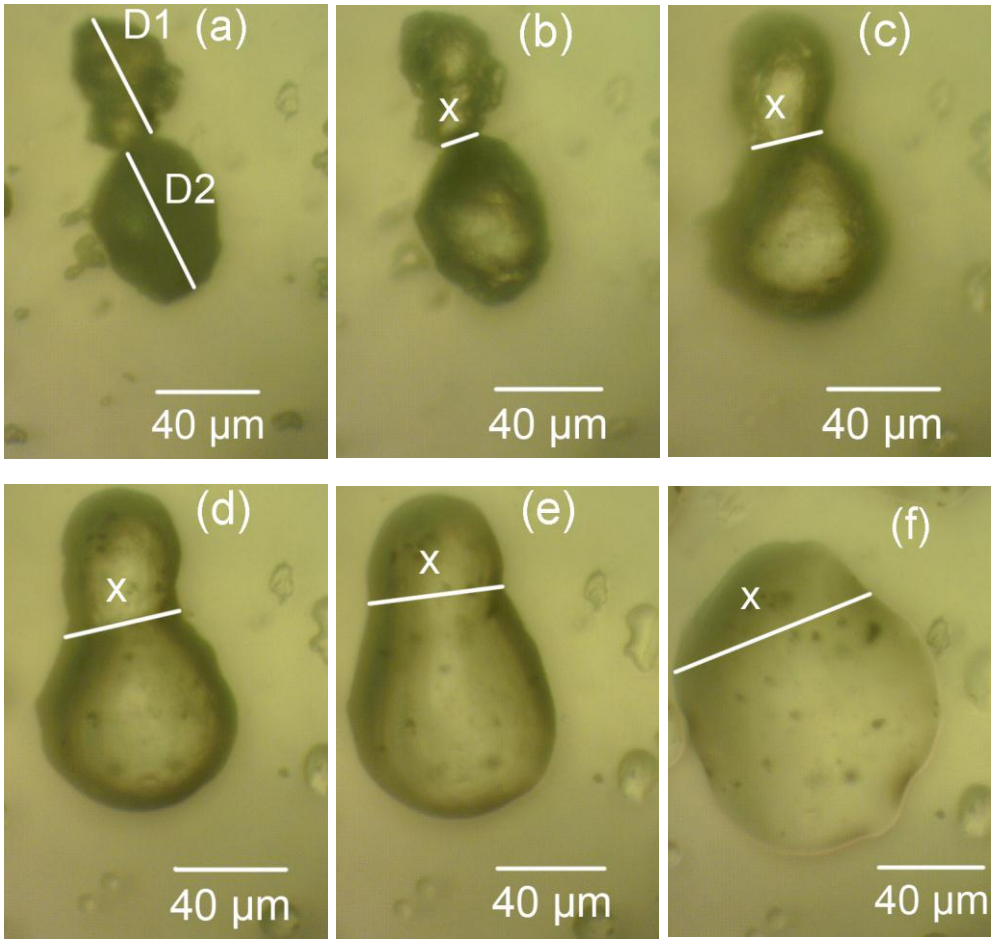

Fig 4. Particle coalescence of 1 wt% GNP/PEEK particles mixed by wet method: (a) Room temperature, (b-f) during coalescence in the temperature ranging from 340 to 400 °C. D1 and D2 are particle diameters, D is (D1+D2)/2, and x is the neck length.

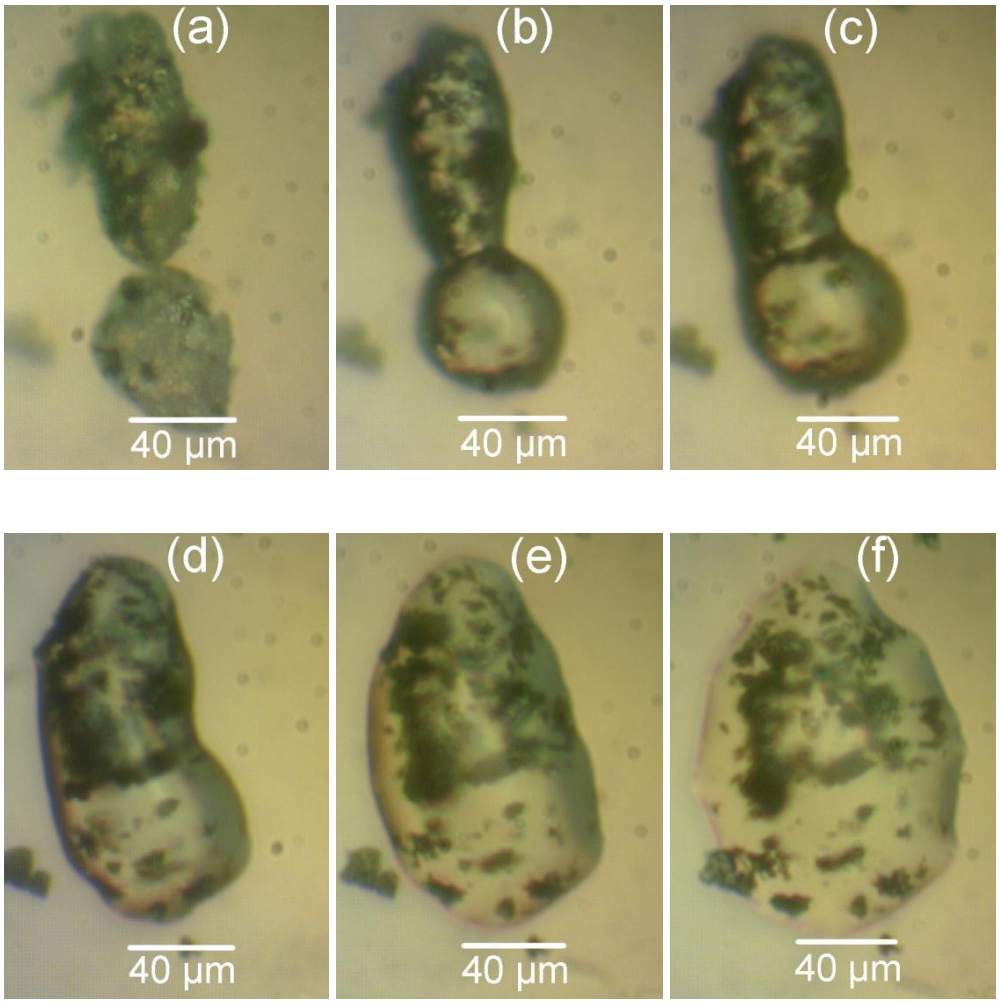

Fig 5. Particle coalescence of 10 wt% GNP/PEEK particles mixed by wet method: (a) Room temperature, (b-f) during coalescence in the temperature ranging from 340 to 400 ºC.

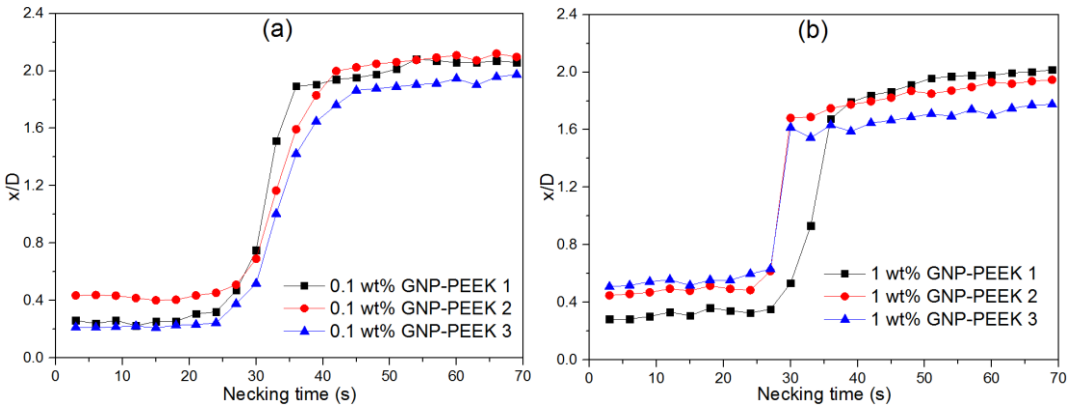

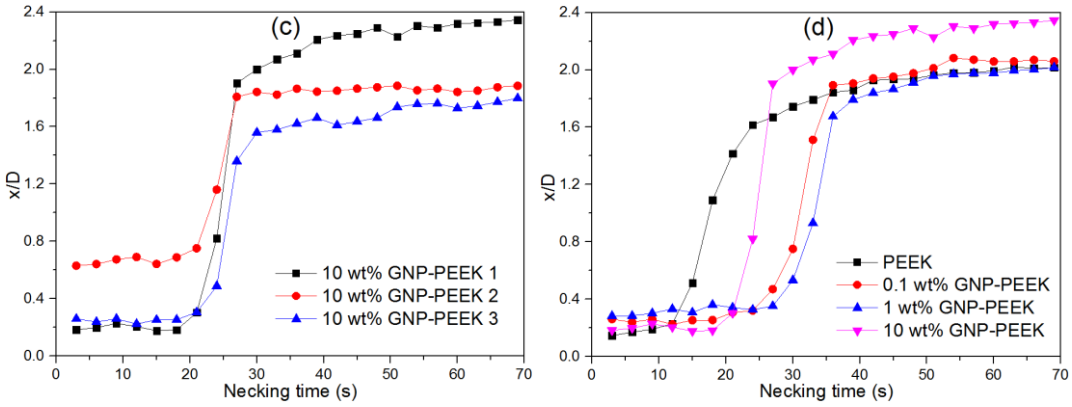

Fig 6. Coalescence results of (a) 0.1 wt% GNP/PEEK; (b) 1 wt% GNP/PEEK; (c) 10 wt% GNP/PEEK particles mixed by wet method and their typical curves in (d).

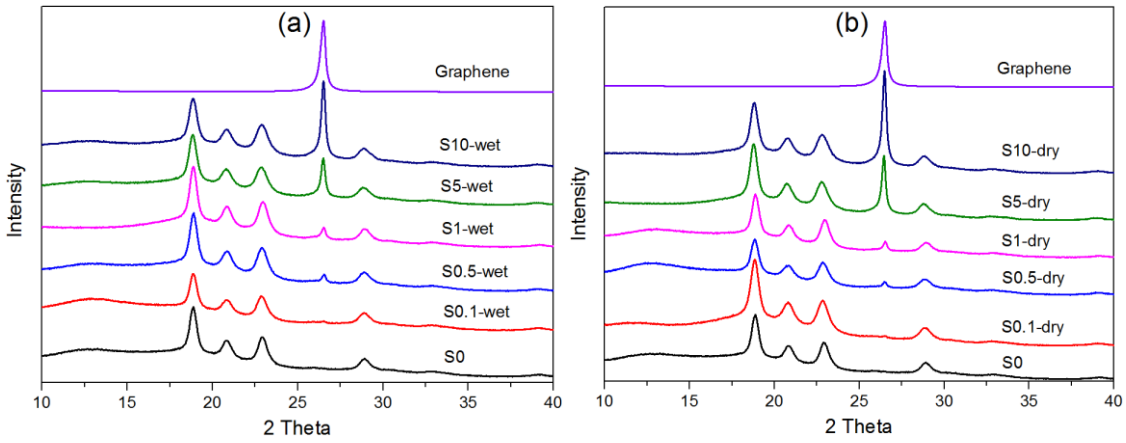

Fig 7. XRD patterns of PEEK, GNP, and GNP-PEEK nanocomposites with different GNP weight percentages using the (a) dry and (b) wet dispersion methods.

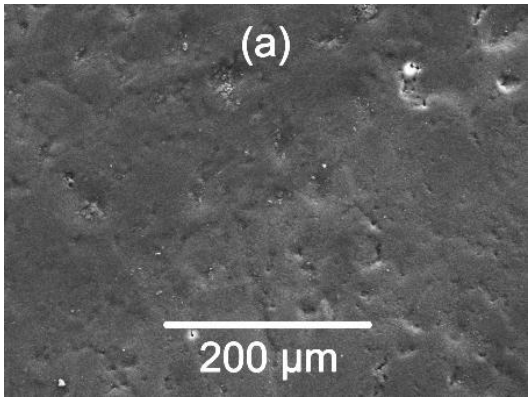

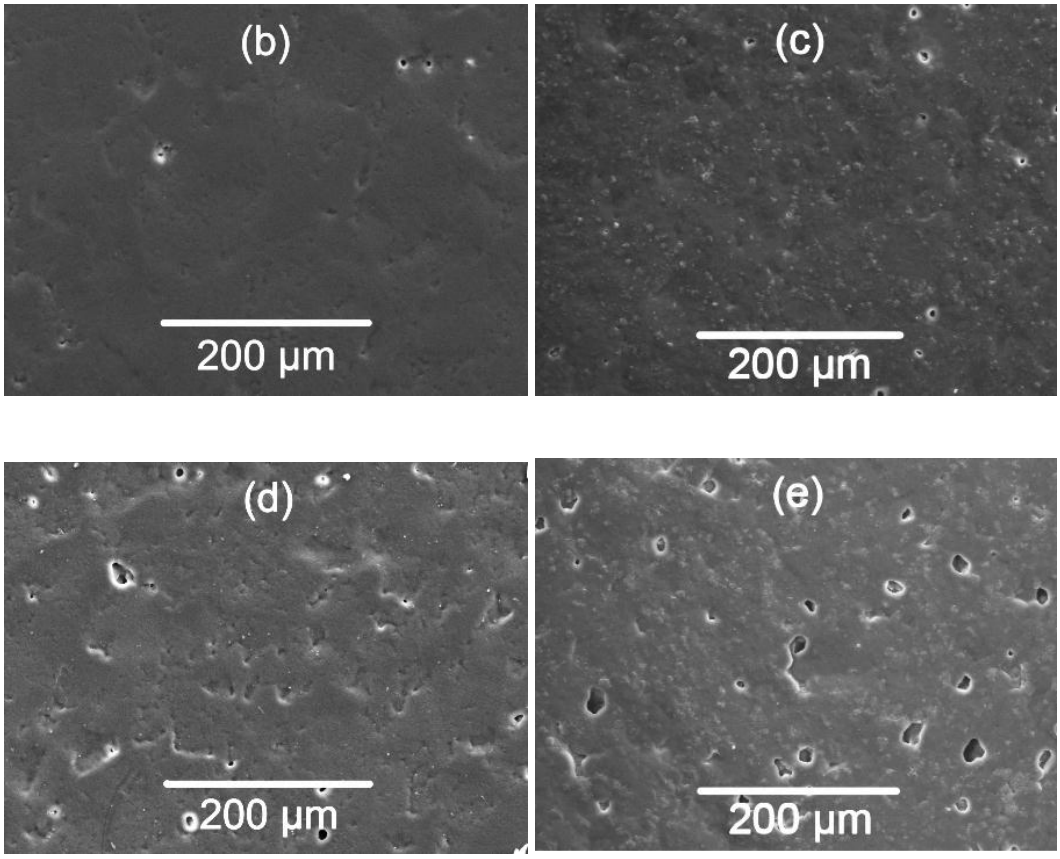

Fig 8. The morphology of flat film surface of (a) S0, (b) S0.1-wet, (c) S1-wet, (d) S0.1-dry, and (e) S1-dry

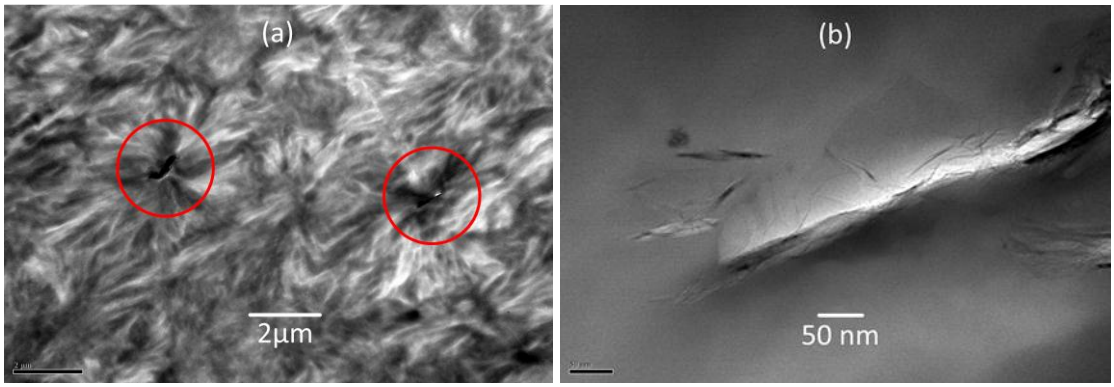

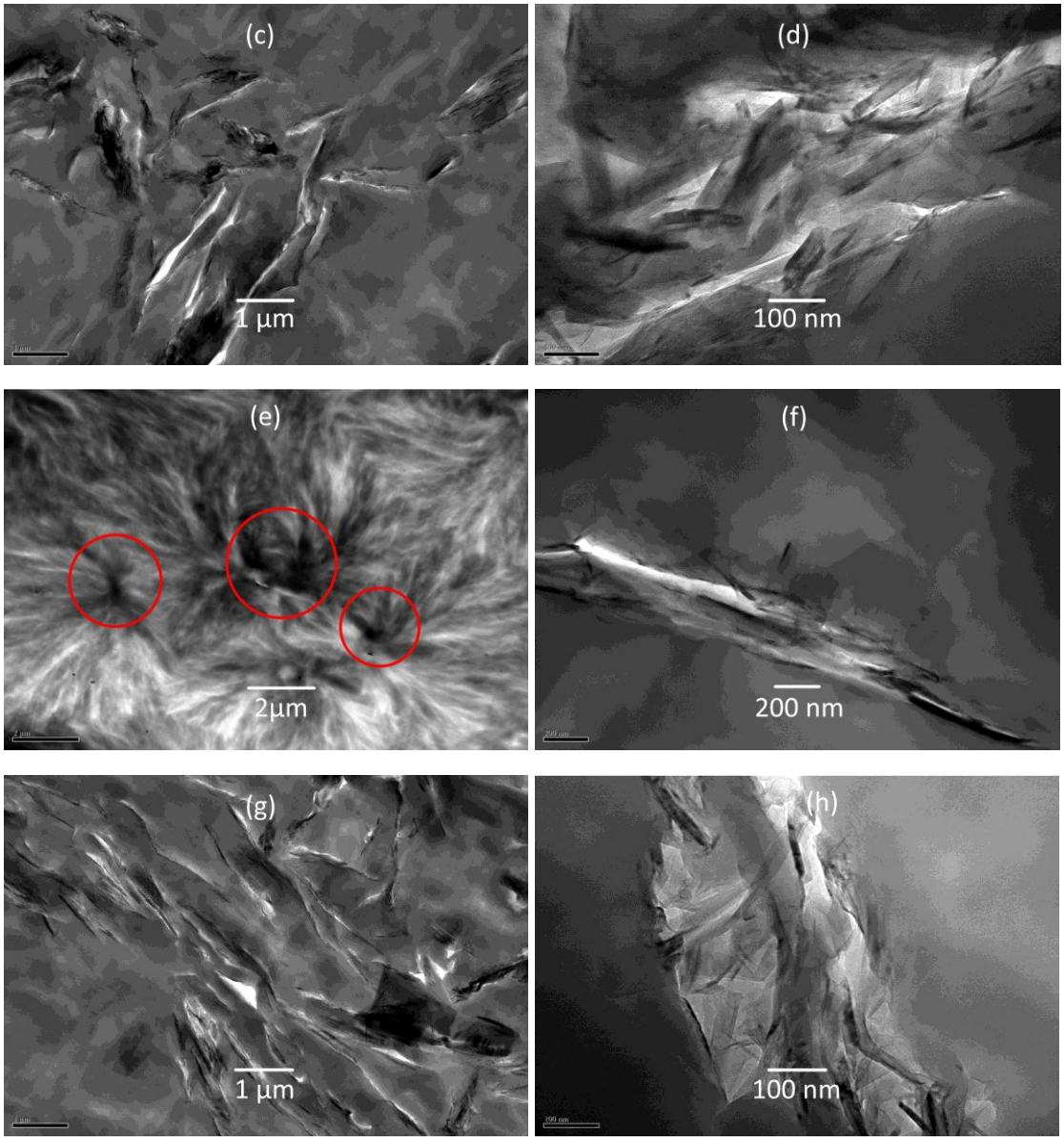

Fig 9. TEM images of cross-section area of (a, b) S0.1-wet, (c, d) S5-wet, (e, f) S0.1-dry, (g, h) S5-dry under low and high magnifications

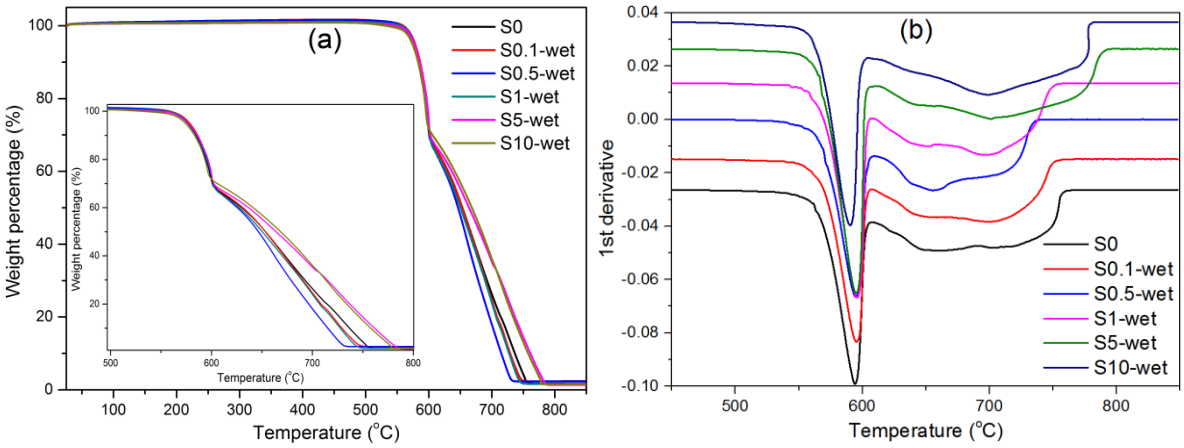

Fig 10. (a) TGA data in air and (b) their 1st derivative curves for S0, S0.1-wet, S0.5-wet, S1-wet, S5-wet and S10-wet.

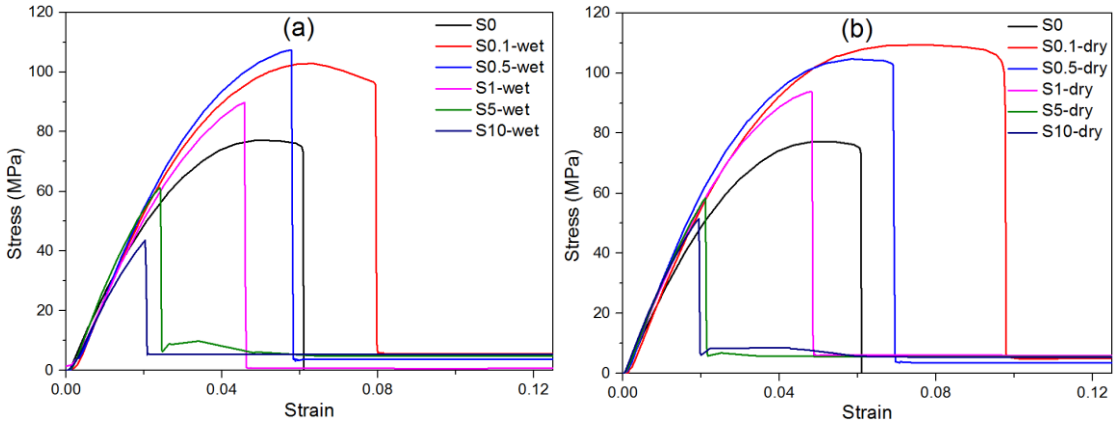

Fig 11. Typical strain-stress of PEEK and GNP-PEEK films with: (a) wet powder mixing method, and (b) dry powder mixing method

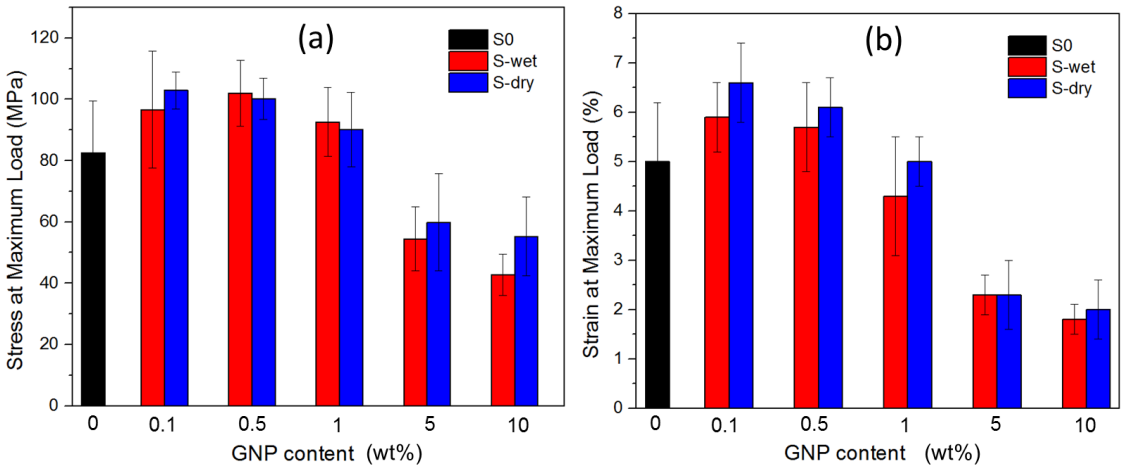

Fig 12. (a) Stress at Maximum Load and (b) Strain at Maximum load for the GNP/PEEK composites films obtained using the dry and wet solution methods.

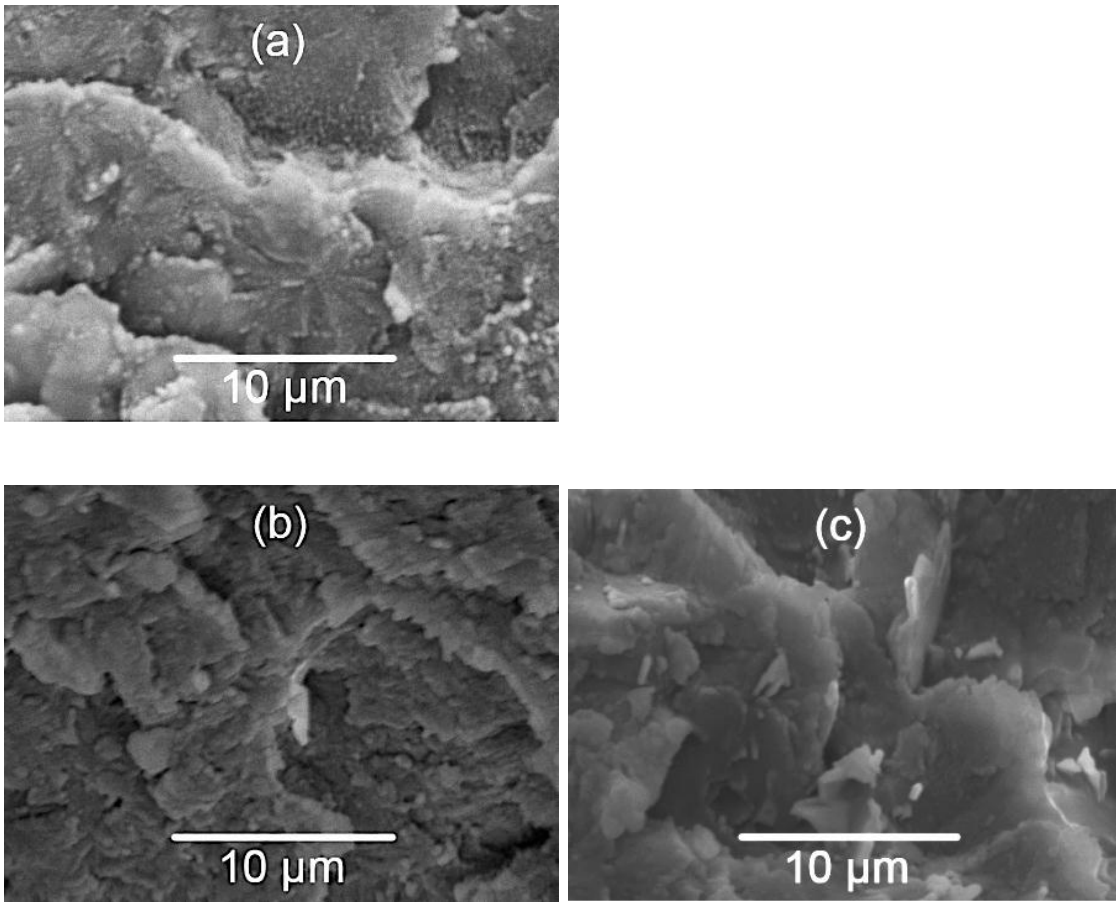

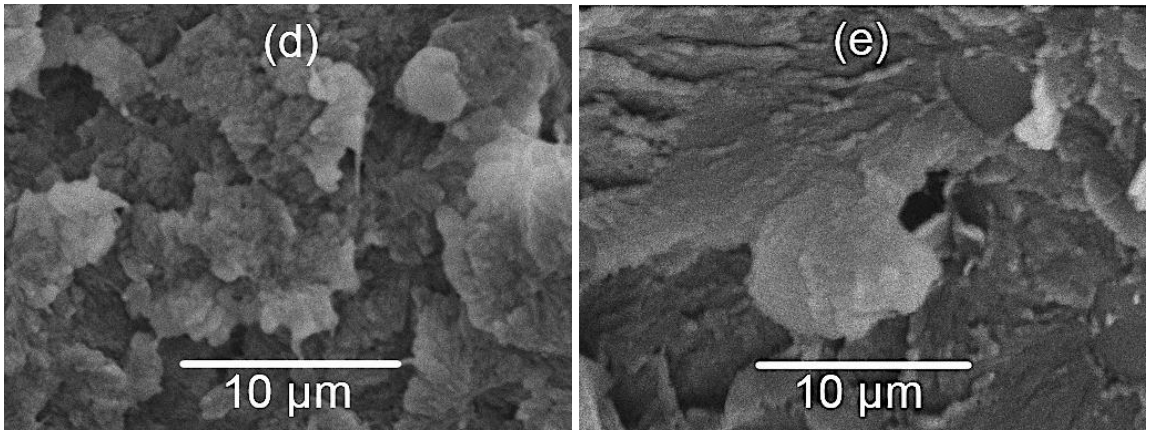

Fig 13. SEM images of fractured surface: (a) S0, (b) S0.1-wet, (c) S1-wet, (d) S0.1-dry, (e) S1-dry

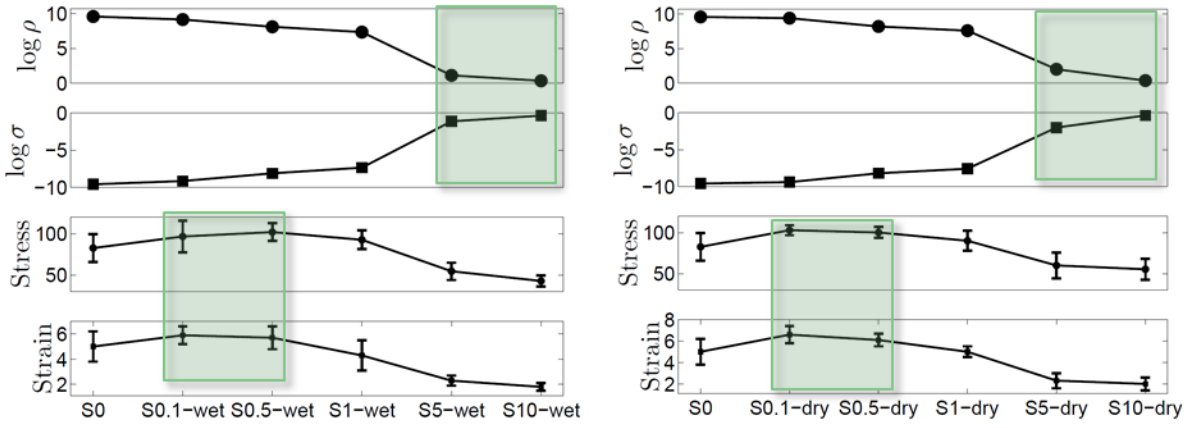

Fig 14. Combination of electrical resistivity (Ω·m), electrical conductivity (S/m), stress at maximum load (MPa), and strain at maximum load (%) for the samples manufactured using the wet (A) and dry (B) dispersion methods.

Table 1. R_a values of plain PEEK (S0), S0.1-wet, and S1-wet

	Plain PEEK (S0)	S0.1-wet	S1-wet
R_a (μm)	3.36 ± 0.23	1.41 ± 0.17	2.65 ± 0.13

Table 2. Electrical resistivity and conductivity of the GNP/PEEK composites films

Film	Electrical resistivity, ρ (Ω·m)	Electrical conductivity, σ (S/m)
S0	$3.9 \pm 1.4 * 10^{9}$	$2.5 \pm 0.9 * 10^{-10}$
S0.1-wet	$1.4 \pm 0.2 * 10^{9}$	$7.1 \pm 1.1 * 10^{-10}$
S0.5-wet	$1.3 \pm 0.1 * 10^{8}$	$7.7 \pm 0.6 * 10^{-9}$
S1-wet	$2.2 \pm 0.2 * 10^{7}$	$4.5 \pm 0.4 * 10^{-8}$
S5-wet	$1.3 \pm 0.1 * 10$	$7.7 \pm 0.6 * 10^{-2}$
S10-wet	2.2 ± 0.1	$4.5 \pm 0.2 * 10^{-1}$
S0.1-dry	$2.5 \pm 0.2 * 10^{9}$	$4.0 \pm 0.3 * 10^{-10}$
S0.5-dry	$1.6 \pm 0.2 * 10^{8}$	$6.2 \pm 0.8 * 10^{-9}$
S1-dry	$3.9 \pm 1.5 * 10^{7}$	$2.6 \pm 0.1 * 10^{-8}$
S5-dry	$9.9 \pm 1.5 * 10$	$1.0 \pm 0.2 * 10^{-2}$
S10-dry	2.3 ± 0.1	$4.3 \pm 0.2 * 10^{-1}$